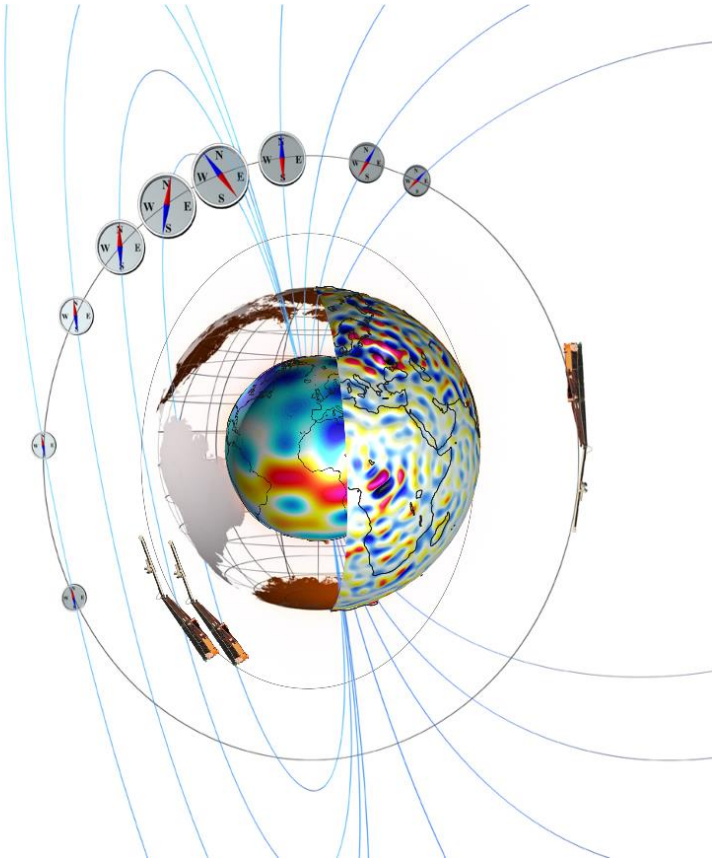
Data, Innovation, and Science Cluster

Swarm-ULF Description of the Processing Algorithm



Doc. no: SW-TN-EPSS-GS-001_ULF_DPA, Rev: 0, 15 Apr 2024

Prepared:		Checked:	
Balazs Heilig	Date 15 Apr 2024	Tamás Bozóki	Date 15 Apr 2024
Team Leader		Scientist	
Approved:			

© EPSS, Hungary, 2024. Proprietary and intellectual rights of EPSS, Hungary are involved in the subject-matter of this material and all reproduction, use, disclosure, and sales rights pertaining to such subject-matter are expressly reserved.

This document is released for use only if signed by the Project Manager or the Team Leader.

Record of Changes

Reason	Description	Rev	Date
Initial version	Released.	0	15 Apr 2024

The use and/or disclosure, etc. of the contents of this document (or any part thereof) is subject to the restrictions referenced on the front page.

Table of Contents

1 Introduction 8
1.1 Scope and applicability 8
2 Applicable and Reference Documentation 8
2.1 Applicable Documents 8
2.2 Reference Documents 8
2.3 Abbreviations 10
3 Scientific and Technical Background 12
3.1 ULF waves 12
3.1.1 Pc 2-3-4 waves 13
3.1.2 Pi2 waves 13
3.1.3 Pc1 waves 14
3.2 Previous attempts 14
4 Algorithms Description 16
4.1 ULF wave detection 16
4.1.1 Reading the data 16
4.1.2 Pre-processing 16
4.1.2.1 Interpolating missing and flagged values 16
4.1.2.2 Transforming the magnetometer data into a mean field-aligned system 16
4.1.2.3 Removal of the mean field 18
4.1.2.4 Calculation of auxiliary data 18
4.1.3 Derivation of the one-minute resolution characterisation 18
4.1.3.1 Calculation of the Pc2, Pc3, Pc4 and Pi2 activity indices 18
4.1.3.2 Calculation of the rms of FAC 19
4.1.3.3 Calculation of the dominant frequency 19
4.1.3.4 Calculation of one-minute means of position and time 22
4.1.3.5 Flag definitions 22
4.1.3.6 Product variables 23
4.1.4 Main steps of the detection process 24
4.1.4.1 Segmentation of the data into quarter of half orbits 24
4.1.4.2 Analysis of a pole-to-pole profile – calculation of spectra, coherence and phase difference 25
4.1.4.3 Wave event detection 25
4.1.4.4 Product variables 27

The use and/or disclosure, etc. of the contents of this document (or any part thereof) is subject to the restrictions referenced on the front page.

4.1.4.5 Calculation of event mean properties 28
4.1.4.6 Product variables 28
4.1.4.7 Saving the data in daily cdf product files 30
4.2 Pc1 wave detection 30
4.2.1 Reading the data 30
4.2.2 Pre-processing 31
4.2.2.1 Calculation of auxiliary data 31
4.2.2.2 Segmentation of the data into half orbits 33
4.2.2.3 Transforming the high-frequency magnetic measurements into a field-aligned coordinate system 33
4.2.2.4 Removal of the mean field 33
4.2.3 Main steps of the detection process 34
4.2.3.1 Determining spectrograms and noise removal 34
4.2.3.2 Pc1 candidate event search based on peak finding and coherence 34
4.2.3.3 Identifying and extracting individual Pc1 events 34
4.2.3.4 Quality flags characterizing spectral peaks 35
4.2.3.5 Product variables characterizing spectral peaks 35
4.2.3.6 Quality flag characterizing individual Pc1 events 37
4.2.3.7 Product variables characterizing the mean properties of the identified Pc1 events 38
4.2.3.8 Saving the data in daily cdf product files 40
4.2.3.9 No event case 40
Summary 41

List of Figures

Figure 1, Flowchart showing the main steps of ULF detection. 17

Figure 2, A visualisation example of the ULF wave product parameters (Swarm A, March 18, 2015 03:00-03:38 UT, MLT = 07). (1st) high-pass (f_c at 12 mHz) filtered $\boldsymbol{dBp}$, (2nd) $\boldsymbol{dBp}$ filtered in the Pc3 band (blue), Pc3 act(ivity) (dashed magenta), FAC (red), AOB (vertical cyan), (3rd) $\boldsymbol{dBp}$ filtered in the Pi2 band (light blue), flag_EPB (blue), IBI index (red), (4th) wavelet spectrogram of $\boldsymbol{dBp}$ (background), detected potential wave events (black), dominant frequency (red dots), and plasmapause location proxy (dashed blue), (5th) wavelet spectrogram of electron density fluctuations. 20

Figure 3, Same as Figure 2 but for 12:27-13:06 UT, MLT = 7.8. 21

Figure 4, Peak detection threshold as a function of frequency 26

Figure 5, Half width (called width in this figure) is defined at half of the peak prominence (an artificial example curve composed of a full period cosine and six Gaussian). 26

Figure 6, Flowchart showing the main steps of Pc1 event detection 32

The use and/or disclosure, etc. of the contents of this document (or any part thereof) is subject to the restrictions referenced on the front page.

Figure 7 A visualisation example of the noise removal procedure for the 30th half orbit on 18 March, 2015. The first, second and third columns show the spectrograms of the Bp, Ba and Br components of the fluctuation magnetic field, respectively. The top, middle and bottom rows correspond to the original, raw spectrograms (top), to the spectrograms from where 1/f type and narrowband noises had been removed (middle), and to the final, smoothed spectrograms. See the text for more details..... 33

Figure 8, A visualisation example of events identified in the Br component for the 30th half orbit on 18 March, 2015. The top figure shows the original, raw spectrogram, while the bottom figure shows those areas of the spectrogram that correspond to the identified two Pc1 events..... 35

List of Tables

Table 1, Morphological classification of geomagnetic pulsations..... 12

Table 2, Filter corner frequencies (periods)..... 18

The use and/or disclosure, etc. of the contents of this document (or any part thereof) is subject to the restrictions referenced on the front page.

1 Introduction

1.1 Scope and applicability

This document comprises the description of the processing algorithms of the Swarm Level 2 (L2) ULF products in response to the requirements of [AD-1]. Swarm ULF includes the following two products [AD-2]:

- **ULFxMAG_2F** – Characterisation of Pc4, Pc3, Pc2 and Pi2 ULF wave activity based on MAGx_LR observations
- **PC1xMAG_2F** – Characterisation of Pc1 (EMIC) ULF wave activity based on MAGx_HR observations

The Swarm-ULF Product Definition document [AD-2] is available in the SVN folder: https://smart-svn.space-center.dk/svn/smart/SwarmDISC/DISC_Projects/?????????/Deliverables/.

Current or updated version of this document is available in the SVN folder: https://smart-svn.space-center.dk/svn/smart/SwarmDISC/DISC_Projects/?????????/Deliverables/.

2 Applicable and Reference Documentation

2.1 Applicable Documents

The following documents are applicable to the definitions within this document.

[AD-1] SW-OF-DTU-GS-010, rev 2 – Subcontractor's section 2.1.23, Swarm DISC-4 Proposal.

[AD-2] SW-TN-EPSS-GS-001_ULF_PDD_i1r0, Swarm-ULF Product Definition Document.

[AD-3] SW-RS-DSC-SY-0007 – Swarm Level 1b Product Definition.

[AD-4] SW-DS-DTU-GS-0001, rev 3 – Swarm Level 2 Processing System, Product specification for L2 Products and Auxiliary Products

2.2 Reference Documents

The following documents contain supporting and background information to be taken into account during the activities specified within this document.

[RD-1] Nakariakov, V., V.A. Pilipenko, B. Heilig, P. Jelínek, M. Karlický, D.Y. Klimushkin, D.Y. Kolotkov, D.-H. Lee, G. Nisticò, T. Van Doorsselaere, G. Verth, I.V. Zimovets, Magnetohydrodynamic Oscillations in the Solar Corona and Ultra-Low Frequency Oscillations in the Earth's Magnetosphere: Towards Consolidated Understanding (2016), Space Science Reviews 200, 75-203, doi: 10.1007/s11214-015-0233-0.

[RD-2] Heilig B., H. Lühr, M. Rother (2007) Comprehensive study of ULF upstream waves observed in the topside ionosphere by CHAMP and on the ground. Annales Geophysicae, 25, 737-754, 2007.

[RD-3] Heilig B., P. R. Sutcliffe (2016) Coherence and phase structure of compressional ULF waves at low-Earth-orbit observed by the Swarm satellites, Geophys. Res. Let. 43, 945-951, doi:10.1002/2015GL067199.

[RD-4] Thomas, N., Vichare, G. & Sinha, A.K. (2016) Spatial frequencies associated with the latitudinal structures of ionospheric currents seen by CHAMP satellite. Astrophys Space Sci 361, 205. https://doi.org/10.1007/s10509-016-2787-z.

The use and/or disclosure, etc. of the contents of this document (or any part thereof) is subject to the restrictions referenced on the front page.

[RD-5] Sutcliffe, P. R., and Lühr, H. (2003), A comparison of Pi2 pulsations observed by CHAMP in low Earth orbit and on the ground at low latitudes, Geophys. Res. Lett., 30, 2105, doi:10.1029/2003GL018270, 21.

[RD-6] Vellante, M., et al. (2004), Ground/satellite signatures of field line resonance: A test of theoretical predictions, J. Geophys. Res., 109, A06210, doi:10.1029/2004JA010392.

[RD-7] Heilig B., P. R. Sutcliffe, D. C. Ndiitwani, A. Collier (2013) Statistical study of geomagnetic field line resonances observed by CHAMP and on the ground, J. Geophys. Res. Space Physics, 118, 1934-1947, doi: 10.1002/jgra.50215.

[RD-8] Yagova, N. V., B. Heilig, and E. N. Fedorov (2015) Pc2-3 geomagnetic pulsations on the ground in the magnetosphere, and in the ionosphere. MM100, CHAMP and THEMIS observations, Ann. Geophys., 33, 117-128, doi:10.5194/angeo-33-117-2015.

[RD-9] Cuturrufo, F., V. Pilipenko, B. Heilig, M. Stepanova, H. Lühr, P. Vega, A. Yoshikawa (2015) Near-equatorial Pi2 and Pc3 waves observed by CHAMP and on SAMBA/MAGDAS stations, Advances in Space Research 55 1180–1189, doi:10.1016/j.asr.2014.11.010.

[RD-10] Heilig, B., S. Lotz, J., Verő, P. Sutcliffe, J. Reda, K. Pajunpää, and T. Raita (2010) Empirically modelled Pc3 activity based on solar wind parameters. Annales Geophysicae, 28, 1703–1722, 2010.

[RD-11] Pilipenko, V., E. Fedorov, B. Heilig, M. J. Engebretson (2008) Structure of ULF Pc3 waves at low latitudes, J. Geophys. Res. 113 (2008), A11208, doi:10.1029/2008JA013243.

[RD-12] Balasis, G., Papadimitriou, C., Daglis, I. A., and Pilipenko, V. (2015) ULF wave power features in the topside ionosphere revealed by Swarm observations, Geophys. Res. Lett., 42, 6922–6930, doi:10.1002/2015GL065424.

[RD-13] Thomas, N., Shiokawa, K., & Vichare, G. (2019) Comprehensive study of low-latitude Pi2 pulsations using observations from multisatellite Swarm mission and global network of ground observatories. Journal of Geophysical Research: Space Physics, 124, 1966–1991. https://doi.org/10.1029/2018JA026094

[RD-14] Park, J.-H., Kim, K.-H., Kwon, H.-J., Jee, G., & Hwang, J. (2020) A statistical study of Pi2 pulsations observed in the upper ionosphere using Swarm magnetic field data. Journal of Geophysical Research: Space Physics, 125, e2019JA027293. https://doi.org/10.1029/2019JA027293.

[RD-15] Martines-Bedenko, V.A., Pilipenko, V.A., Fedorov, E.N. et al. (2020) Low-Latitude Pi2 Waves according to Observations on SWARM Satellites and Ground Stations. Cosmic Res 58, 1–11. https://doi.org/10.1134/S0010952520010050

[RD-16] Allen, R. C., J.-C. Zhang, L. M. Kistler, H. E. Spence, R.-L. Lin, B. Klecker, M. W. Dunlop, M. André, and V. K. Jordanova (2015) A statistical study of EMIC waves observed by Cluster: 1. Wave properties. J. Geophys. Res. Space Physics, 120, 5574–5592. https://doi.org/10.1002/2015JA021333

[RD-17] Kim, H., Hwang, J., Park, J., Bortnik, J., &Lee, J. (2018) Global characteristics of electromagnetic ion cyclotron waves deduced from Swarm satellites. Journal of Geophysical Research: Space Physics,123, 1325–1336. https://doi.org/10.1002/2017JA024888

[RD-18] Kim, H., Shiokawa, K., Park, J., Miyoshi, Y., Stolle, C., & Buchert, S. (2021) Statistical analysis of Pc1 wave ducting deduced from Swarm satellites. Journal of Geophysical Research: Space Physics, 126, e2020JA029016. https://doi.org/10.1029/2020JA029016

The use and/or disclosure, etc. of the contents of this document (or any part thereof) is subject to the restrictions referenced on the front page.

[RD-19] Li, W., and Hudson, M. K. (2019) Earth's Van Allen radiation belts: From discovery to the Van Allen Probes era. J. Geophys. Res. Space Physics, 124, 8319–8351. https://doi.org/10.1029/2018JA025940

[RD-20] Park, J., Lühr, H., and Rauberg, J. (2013) Global characteristics of Pc1 magnetic pulsations during solar cycle 23 deduced from CHAMP data. Ann. Geophys., 31, 1507–1520. https://doi.org/10.5194/angeo-31-1507-2013

[RD-21] Saikin, A. A., Zhang, J.-C.; Allen, R. C.; Smith, C. W.; Kistler, L. M.; Spence, H. E. et al. (2015) The occurrence and wave properties of H+-, He+-, and O+-band EMIC waves observed by the Van Allen Probes. J. Geophys. Res. Space Physics, 120, 7477–7492. https://doi.org/10.1002/2015JA021358

[RD-22] Wang, Y., Li, Y., Liu, K., Song, W., Xiong, Y., and Yao, F. (2023) Statistical analysis of electromagnetic ion cyclotron rising-tone emissions based on deep learning. J. Geophys. Res. Space Physics, 128, e2022JA031085. https://doi.org/10.1029/2022JA031085

2.3 Abbreviations

A list of acronyms and abbreviations used by Swarm partners can be found here. Any acronyms or abbreviations not found on the online list but used in this document can be found below.

Acronym ***or abbreviation***	***Description***
EMIC	ElectroMagnetic Ion-Cyclotron waves
EPB	Equatorial Plasma Bubble
FAC	Field Aligned Current
KHI	Kelvin-Helmholtz Instability
LP	Langmuir Probe
MFA	Mean-field-aligned
MLT	Magnetic Local Time
Ne	electron number density
NEC	North-East-Centre
Pc	continuous type pulsation (Pc1, Pc2, Pc3, Pc4, Pc5)
Pi	irregular pulsation (Pi1, Pi2)
QD	Quasi-Dipole
R_E	Earth radius, 6371.2 km
RD	Reference Document
rms	root mean square

The use and/or disclosure, etc. of the contents of this document (or any part thereof) is subject to the restrictions referenced on the front page.

Acronym ***or abbreviation***	***Description***
SZA	Solar Zenith Angle
ULF	ultra-low frequency (1 mHz – 5 Hz)

The use and/or disclosure, etc. of the contents of this document (or any part thereof) is subject to the restrictions referenced on the front page.

3 Scientific and Technical Background

3.1 ULF waves

ULF waves are periodic fluctuations of the geomagnetic field with periods ranging from seconds to minutes. They are ubiquitous in the Geospace and solar wind plasma, when observed on the ground they are often referred to as geomagnetic pulsations. The morphological classification of ULF waves was introduced in the 1960s. ULF waves were divided into two large groups, a group of the more regular, sinusoidal fluctuations called continuous pulsations and depicted by Pc, and a group of irregular, impulsive pulsations depicted by Pi. Both groups are further divided into several types based on their wave period. These types are numbered. Larger numbers indicate larger periods. Table 1 lists the pulsation types along with their periods in seconds, their frequency, and typical amplitudes on the ground [RD-1].

Table 1, Morphological classification of geomagnetic pulsations

Pulsations	T, s	f	Amplitudes, nT
Pc 1	0.2–5	0.2–5 Hz	0.01–0.1
Pc 2	5–10	0.1–0.2 Hz	0.1–1
Pc 3	10–45	22–100 mHz	1–10
Pc 4	45–150	7–22 mHz	5–50
Pc 5	150–600	2–7 mHz	50–500
Pi 1	1–40	0.025–1 Hz	0.2–1
Pi 2	40–150	2–25 mHz	10–100

The various types of ULF waves are driven by different processes. Solar wind flow shear on the magnetosphere flanks generates Kelvin-Helmholtz type waves which propagate inward producing typically Pc4-Pc5 ULF waves. Dayside Pc3s are generated in the Earth's ion foreshock via ion-cyclotron resonance and swept into the magnetosphere by the solar wind [RD-2].

Not all types of ULF waves can be detected clearly at LEO. Detectability depends first on the wave period. During 2.5-10 minutes, the period of a Pc5 wave, Swarm covers 10°- 40° in latitude range, which may include low and high latitudes, or even dayside and nightside high latitudes. Pc5 waves are hardly ever observed at low latitudes. Another difficulty is the satellite speed. Quasi-static magnetic structures at various spatial scales (plasma bubbles, crustal field anomalies, electrojets, field-aligned currents) show up in the recorded data as fluctuations at various frequencies in the ULF band. Equatorial and auroral electrojets as sampled on Swarm orbit, have frequency components up to around 10 mHz [RD-4]. Crustal field anomalies contaminate the Pi2, and the Pc3-4 bands [RD-5], while auroral field-aligned currents are observed as broad-band bursts [RD-2]. When characterising ULF wave phenomena observed at polar LEO, we need to pay attention to all these phenomena not to confuse them with ULF waves. That is why we need to limit the wave identification spatially to lower than polar latitudes and in frequency to higher than 12 mHz. Besides, crustal field anomalies up to 110 harmonic degrees which correspond to ca. 390 km wavelength or 50 s period (satellite speed is 7.6 km/s), can be removed by using the CHAOS-7 magnetic field model. Thus, Pi2 and Pc4 waves can be cleaned from their contribution to the observed signal.

Cold plasma ULF waves are either propagating waves in shear Alfvén mode or compressional mode or standing waves of the same wave modes [RD-1]. Shear Alfvén mode propagates along field lines, and the corresponding resonances are formed also along field lines. The frequency of field line resonances changes with latitude (primarily due to the varying field line length), and resonance shells are very narrow, typically a few tens of kms. Swarm traverses the resonance shells within a few seconds, at which point it encounters a

The use and/or disclosure, etc. of the contents of this document (or any part thereof) is subject to the restrictions referenced on the front page.

different resonance with a distinct frequency and phase. Moreover, the phase changes very rapidly by 180°within the narrow resonance. This results in a strong Doppler shift [RD-6][RD-7]. All these circumstances make the direct observation of field line resonances at polar LEO practically impossible. Propagating Alfvén waves are also observed with a strong Doppler shift at midlatitudes due to the mutual relation of the wave vector and the satellite motion direction. On the other hand, waves with long coherence length propagating vertically, such as dayside Pc3s, can be safely detected [RD-2], [RD-3]. Similarly, nightside Pi2s, signatures of a compressional mode resonance standing in the vertical direction, i.e., with phase fronts roughly parallel with the spacecraft orbit or the ionosphere are also observed without Doppler shift. Pc2 waves are observed rarely [RD-8]. On the dayside, they are simply the higher frequency extension of Pc3 waves. Pc1 waves are the only transversal waves that can be detected safely by polar LEO satellites thanks to their higher frequency (shorter wave period) [RD-18].

The Swarm-ULF products [AD-2] contribute to the monitoring of physical processes taking place in the top-side ionosphere.

3.1.1 Pc 2-3-4 waves

The dominant sources of Pc2-4 wave activity in the magnetosphere are 1) foreshock upstream waves [RD-2], 2) Kelvin-Helmholtz instability (KHI) and 3) field line resonances [RD-6][RD-7]. Magnetospheric waves of upstream origin are typically dayside Pc3 waves propagating as compressional waves Earthward from the foreshock source region. The magnetosphere is focusing them at low latitudes, thus, they peak near the geomagnetic equator before noon (MLT) [RD-2][RD-10][RD-11]. Approaching Earth, they reach a point where they are reflected back (turning point), below this altitude they are observed as the exponentially decaying evanescent field of the reflected wave. Due to their ion-cyclotron origin [RD-2], their frequency (f) is directly proportional to the magnitude of the interplanetary magnetic field (B_{imf}) [RD-7], so that in the magnetosphere or on the ground

$$f\ [\mathrm{mHz}] \approx 6 \cdot B_{imf}[\mathrm{nT}].$$

Since, the median interplanetary magnetic field magnitude is around 5 nT, upstream waves typically produce Pc3 waves [RD-1][RD-2]. However, when B_{imf} drops below ~4 nT or increases higher than ~16 nT, the resulting waves will fall into the Pc4 or Pc2 range. The amplitude of ULF waves of upstream origin is controlled by the solar wind speed and the direction of the interplanetary magnetic field [RD-10].

KHI is an important source of Pc5 wave activity in the dawn and dusk sectors, as the flow shear driving them maximises at the flanks of the magnetosphere. KHI drives surface waves on the magnetopause, the associated magnetospheric waves decay exponentially towards the Earth [RD-1]. KHI-associated magnetospheric waves are Pc5-Pc4 waves peaking at higher L-shells (higher latitudes on the ground).

Both these waves couple to shear-Alfvén-mode field line resonances (FLRs) wherever their frequency matches the eigenfrequency of the encountered field line [RD-7]. The FLR frequency depends on the field line length (magnetic latitude) and the plasma mass density along the field line. Consequently, the resonance frequency decreases toward higher latitudes (except for near the plasmapause), while at a given location, the frequency is controlled primarily by geomagnetic activity-dependent plasma density.

3.1.2 Pi2 waves

Pi2 waves are associated with substorm activity [RD-1], [RD-5]. Pi2 waves are believed to be the cavity mode resonance of the compressional mode, standing between the plasmapause and the underlying ionosphere. Their appearance is closely related to substorm onsets that is why they can be used to detect these onsets.

The use and/or disclosure, etc. of the contents of this document (or any part thereof) is subject to the restrictions referenced on the front page.

The source of the cavity mode is the substorm dynamics (breaking the bursty flow of plasma accelerated toward the Earth). The frequency of Pi2s is determined by the properties of the cavity that is why they show up in a well-defined frequency band. Since the nightside boundaries of this cavity are far from perfect reflectors, the resonance decays within a few cycles. That is the cause of the impulsive (Pi) appearance of these waves.

3.1.3 Pc1 waves

Pc1 pulsations cover the 0.2-5 Hz frequency range. This frequency range is generally accepted to include waves that are referred to as electromagnetic ion cyclotron (EMIC) waves based on their excitation mechanism and the corresponding compressional wave activity. The excitation of EMIC waves requires an anisotropic distribution of energetic (~10-100 keV) protons, large plasma density and a local minimum in the magnetic field, which results in EMIC waves mainly originating in the equatorial inner magnetosphere, but EMIC source regions also exist outside the magnetic equator at higher L-shells in the dayside magnetosphere [RD-16]. In general, EMIC waves are generated as transverse, left-handed polarized waves, consistent with the direction of ion gyration, and reach the ionosphere by propagating along the geomagnetic field lines. In the ionosphere the initially transverse waves also generate compression waves, which can propagate long distances across magnetic field lines parallel to the Earth's surface [RD-18]. Statistical studies indicate that in the topside ionosphere EMIC waves are detected with a peak occurrence rate at midlatitude (including subauroral regions) in the dawn sector and occur preferably during the recovery phase of geomagnetic storms [RD-17]. EMIC waves play an important role in the Earth’s magnetosphere, as they can precipitate relativistic electrons from the outer radiation belt and energetic protons from the ring current. Hereby, their observation provides important information about the energy coupling between the ionosphere and the magnetosphere as well as the particle dynamics inside the Earth’s magnetosphere [RD-19].

3.2 Previous attempts

The detection of ULF waves at LEO is challenging and not always possible as explained in Section 3.1.

[RD-12] used the scalar magnetometer data sampled at 1 Hz to detect Pc3 activity. They did not remove a model field but subtracted the low-pass filtered observations from the total field time series. The cutoff of the applied filter was 20 mHz, i.e. ~10% below the traditional Pc3 lower limit. Spectra were calculated applying a continuous (Morlet) wavelet transformation, and event candidates were selected based on a power criterion (> 1/8 nT^2/Hz, which corresponds to ~ 0.35 nT amplitude). These candidates are then tested against a set of further criteria. Events shorter than twice the dominant period or having their dominant peak outside the Pc3 range or having spikes were dropped.

[RD-2] and [RD-3] used the CHAOS magnetic field model to remove crustal field anomalies and also for the definition of the field aligned reference frame. However, these studies aimed at the statistical investigation of dayside Pc3 waves at LEO and not the identification of wave events.

Pi2 waves have been identified in the compressional component, typically aided by the use of some ground reference measurements [RD-5], [RD-13], [RD-14], [RD-15] and/or the AE index.

Attempts to reliably detect Alfvén waves at polar LEO have mostly failed due to the aforementioned reasons. Alfvén waves, both travelling and standing appear with strong Doppler shift [RD-6], [RD-7]in the data with a very short (some 10 kms) along-the-orbit coherence length. Field line resonances were found, however, by applying statistical methods [RD-7].

The use and/or disclosure, etc. of the contents of this document (or any part thereof) is subject to the restrictions referenced on the front page.

A number of previous works have investigated the statistical characteristics of Pc1 events in the high-frequency magnetic measurements of different satellites (e.g., Cluster: [RD-16], CHAMP [RD-20], Van Allen Probes: [RD-21], Swarm: [RD-17]). The high frequency magnetic data are usually transformed first into a field-aligned coordinate system by using a smoothed version of the measured magnetic field and then the Pc1 events searched in the frequency domain. In some works, the Pc1 events were identified by visual inspection [RD-16], [RD-21], whereas in the automated approaches, after smoothing the dynamic spectrum, the events need to meet different criteria for their wave power, bandwidth and duration [RD-17], [RD-20]. The method we followed is based on a new approach in which Pc1 events are found by searching for definite peaks in the spectra. Thus, compared to previous approaches, this procedure can provide the average frequency and prominence of the events, the average power spectral density (PSD) associated with the peak values, as well as the average rate of frequency change which is known as an important parameter characterizing EMIC waves [RD-22]. This approach is also suitable for isolating Pc1 events occurring simultaneously in different frequency bands. Our algorithm also addresses another general shortcoming of previous approaches by removing the 1/f type noise from the spectra (see Section 3.2), and thus performing the event search also in regions (typically at high latitudes) where field-aligned currents strongly contaminate the spectrum (however, the uncertainty of these regions is indicated by a quality flag).

The use and/or disclosure, etc. of the contents of this document (or any part thereof) is subject to the restrictions referenced on the front page.

4 Algorithms Description

The development of the new products is based primarily on historical data. However, we are targeting quasi real-time product provision for space weather monitoring, hence the procedures have to be designed so that the whole processing chain can be executed within a few minutes once new data are available. For both products, the pre-processing begins with the analysis of latitudinal (in QD magnetic latitude sense) profiles of the wave phenomena.

4.1 ULF wave detection

In the following, the ULF wave detection process based on LR magnetometer data (MAGx_LR_1B) data is summarised (see also Figure 1 presenting the process in a flowchart).

4.1.1 Reading the data

Input data (MAGx_LR L1b product in NEC frame) for the day considered are read from the source cdf file. The daily data are complemented by the last segment fragment (from the last magnetic pole crossing) of the previous day, so that the daily data contains complete pole-to-pole orbits. At the same time, the last orbit fragment is dropped since it is to be analysed together with data of the following day. The orbit counter is read from the AUXxORBCNT product files.

EFIx_LP L1b and FACxTMS_2F data for the same day are also read as these data are used to aid the detection process to distinguish ULF waves from quasi-static spatial strictures, such as field aligned currents (FACs) and equatorial plasma bubbles.

4.1.2 Pre-processing

All the input data need some pre-processing before they can be applied for the desired purposes.

4.1.2.1 *Interpolating missing and flagged values*

First, missing (gaps lasting for 10 seconds or less) and flagged values (depending on the flag) are interpolated. For Ne, only values with Flags_Ne below 30 are considered (Table 6-4 in [AD-3]):

10-19 Nominal data, error estimate applies;
20-29 Nominal data, but error estimates do not apply/are not yet determined;

4.1.2.2 *Transforming the magnetometer data into a mean field-aligned system*

The model residuals are then transformed into a mean field aligned (MFA) system. The three components of the MFA point along the magnetic field line (B_p, parallel or compressional component), perpendicular to the plane formed by the *p*-axis and the centre of the Earth pointing eastward (B_a, azimuthal or toroidal component), and inward (B_r, radial or poloidal component), completing the right-handed triad. As an estimate of the mean field the latest CHAOS magnetic field model (currently 7.16) is used. The model field includes the core field, the crustal field (up to 110th degree), as well as the magnetic field of the Ring Current.

The use and/or disclosure, etc. of the contents of this document (or any part thereof) is subject to the restrictions referenced on the front page.

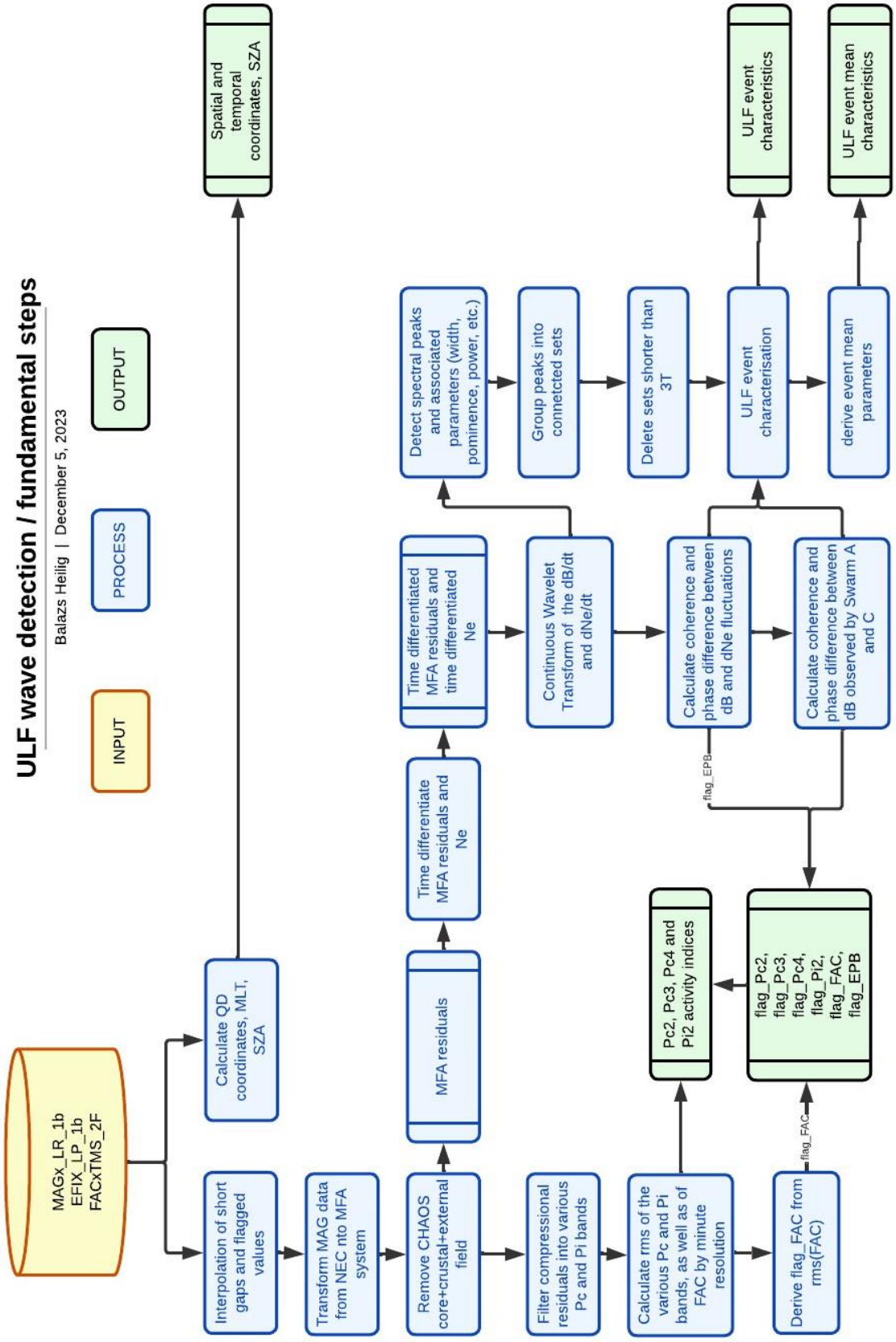


Figure 1, Flowchart showing the main steps of ULF detection.

The use and/or disclosure, etc. of the contents of this document (or any part thereof) is subject to the restrictions referenced on the front page.

4.1.2.3 *Removal of the mean field*

Following the transformation, the mean total field (B_{CHAOS}) is subtracted from the observed field aligned (compressional) component, $dB_p = B_p - B_{CHAOS}$. (Fluctuation of the transverse components hardly contribute to the fluctuation of the total field, as these components are smaller by at least two orders of magnitude). Removal of the crustal field is especially important, as crustal anomalies with down to ~390 km (~110th degree) along-track spatial scales are observed by the satellite moving at a 7.6 km/s speed as fluctuations with periods down to 51 s (or 19.5 mHz). This is already in the Pc3 frequency range. By removing crustal field models, Pi2, Pc4 and Pc3 waves are cleaned from most of the crustal contamination. At even shorter spatial scales, the crustal field anomalies are strongly blurred at Swarm's height due to spatial integration effects.

The transverse components in the MFA system represent the field residuals (dB_a, dB_r) in the corresponding components by definition.

4.1.2.4 *Calculation of auxiliary data*

The calculation of quasi-dipole coordinates, magnetic local time (MLT) and solar zenith angle (SZA) is done for all data points separately. The applied routines are the 'qdipole' routine (written and maintained by N. Olsen, DTU) and the 'solar_zenith_angle' routine (by P. Ritter, GFZ and N. Olsen, DTU).

4.1.3 Derivation of the one-minute resolution characterisation

4.1.3.1 *Calculation of the Pc2, Pc3, Pc4 and Pi2 activity indices*

To calculate Pc2, Pc3, Pc4 and Pi2 activity indices, the compressional residuals are first filtered into the respective frequency bands. The filter applied is a 5th order Butterworth-type bandpass filter with corner frequencies corresponding to the selected band (See Table 2). The filter is applied in a way that it compensates for the time response of the filter (zero-phase filter), so the filtering process does not introduce any phase delay. In the following, the filtered components are depicted by a second lower index referring to the frequency band in question, e.g., $dB_{\theta,Pc3}$.

We note, that the lower cutoff frequency for Pc4 waves is 6.7 mHz (150 s) by definition, however, we raised it to 13.3 mHz (75 s) (Pc4* band). The reason for this is the dayside equatorial electrojets, as well as polar electrojets and FACs that contaminate Swarm data up to ~10 mHz [RD-2], [RD-4].

Table 2, Filter corner frequencies (periods).

Type	lower cutoff frequency (period)	upper cutoff frequency (period)
Pc2	200 mHz (5 s)	100 mHz (10 s)
Pc3	100 mHz (10 s)	22 mHz (45 s)
Pc4*	22 mHz (45 s)	13.3 mHz (75 s)*
Pi2	25 mHz (40 s)	6.7 mHz (150 s)*

The indices are calculated as the root-mean-square (rms) amplitude of the magnetic field fluctuation with one-minute resolution, i.e., in the i-th step, the i-th minute of daily data is taken and the rms of the 60 residuals is calculated as:

$$\mathrm{Pc2}_{\mathrm{act}(i)} = \mathrm{rms}\left(dB_{p,Pc2}(60(i-1)+1{:}60i)\right)\ [\mathrm{in\ pT}],$$

$$\mathrm{Pc3}_{\mathrm{act}(i)} = \mathrm{rms}\left(dB_{p,Pc3}(60(i-1)+1{:}60i)\right)\ [\mathrm{in\ pT}],$$

The use and/or disclosure, etc. of the contents of this document (or any part thereof) is subject to the restrictions referenced on the front page.

$$\mathrm{Pc4}_{\mathrm{act}(i)} = \mathrm{rms}\left(dB_{p,Pc4}(60(i-1)+1{:}\,60i)\right)\ [\mathrm{in\ pT}],$$

$$\mathrm{Pi2}_{\mathrm{act}(i)} = \mathrm{rms}\left(dB_{p,Pi2}(60(i-1)+1{:}\,60i)\right)\ [\mathrm{in\ pT}],$$

where i runs from 1 to 1440 for a single day. Pi2_act is only defined on the night side (SZA>110˘) at low latitudes (< 45°).

4.1.3.2 *Calculation of the rms of FAC*

The rms of FACs are calculated for every minute, analogue to the Pc activity indices. For the i-th minute:

$$\mathrm{FAC}_{\mathrm{act}(i)} = \mathrm{rms}\big(\mathrm{FAC}(60(i-1)+1{:}\,60i)\big)\ [\mathrm{in\ \mu A/m^2}].$$

The rms of FACs are also calculated with higher (1 s) temporal resolution because it is also used for event detection:

$$\mathrm{FAC}_{\mathrm{rms}(j)} = \mathrm{rms}\big(\mathrm{FAC}(j-30{:}\,j+29)\big)\ [\mathrm{in\ \mu A/m^2}].$$

where *j* is now seconds (while i is minutes) and runs from 1 to 86400 for a single day (for this approach, FAC time series has to be complemented with 30 s of the previous and following days).

(Taking every 60th member of the resulting $\mathrm{FAC}_{\mathrm{rms}}$ starting from its 30th member, we obtain a one-minute resolution $\mathrm{FAC}_{\mathrm{act}}$.)

4.1.3.3 *Calculation of the dominant frequency*

The dominant frequency is calculated by means of the continuous wavelet spectra. First, the filtered residual values, e.g., $ddB_{p,Pxn} = dB_{p,Pxn}/dt$, where *x* and *n* stand for the type of the pulsation ('c' or 'i') and the pulsation band ('2', '3', or '4'), respectively, are time differentiated. Then, using the 'Morlet' wavelet as mother wavelet, the continuous wavelet transform (CWT) of the differentiated signal is calculated. The wavelet coefficients are calculated at 24 frequencies per octave in the range 4 mHz - 128 mHz. The dynamic spectra are averaged (using Gaussian weights) for each minute (60 spectra per minute).

The dominant frequency is the spectral peak of the

$$P(\omega) = 2\log_{10}\left|\mathrm{CWT}\left(ddB_{p,Pxn}\right)\right|,$$

i.e., the logarithm of the signal power of the filtered and time-differentiated residual, where ω is the angular frequency ($2\pi f$). Along with the dominant frequency, the prominence, signal power, and the spectral peak half width are also calculated.

The reason for time-differentiating is to reduce the spectral slope thus enhancing the wave-related spectral content with respect to the turbulent background. Time-differentiating corresponds to a scaling of the amplitude by a factor proportional to the frequency, as follows directly from the chain-rule of derivation:

$$\frac{\partial}{\partial t}(A\sin\omega t) = A\omega\cos\omega t.$$

Hence the low-frequency components are suppressed severely, 1/2 per octave, i.e., 1/32 for the lowest frequency considered (4 mHz) compared to the highest (128 mHz).

The dominant frequency and all related characteristics (prominence, signal power, and spectral peak half width) are set to -1, when Flag_FAC>0 or Flag_EPB>0 or when the peak prominence is below 0.6, since in these cases, the observed fluctuation is more likely a spatial structure than some wave phenomenon.

The use and/or disclosure, etc. of the contents of this document (or any part thereof) is subject to the restrictions referenced on the front page.

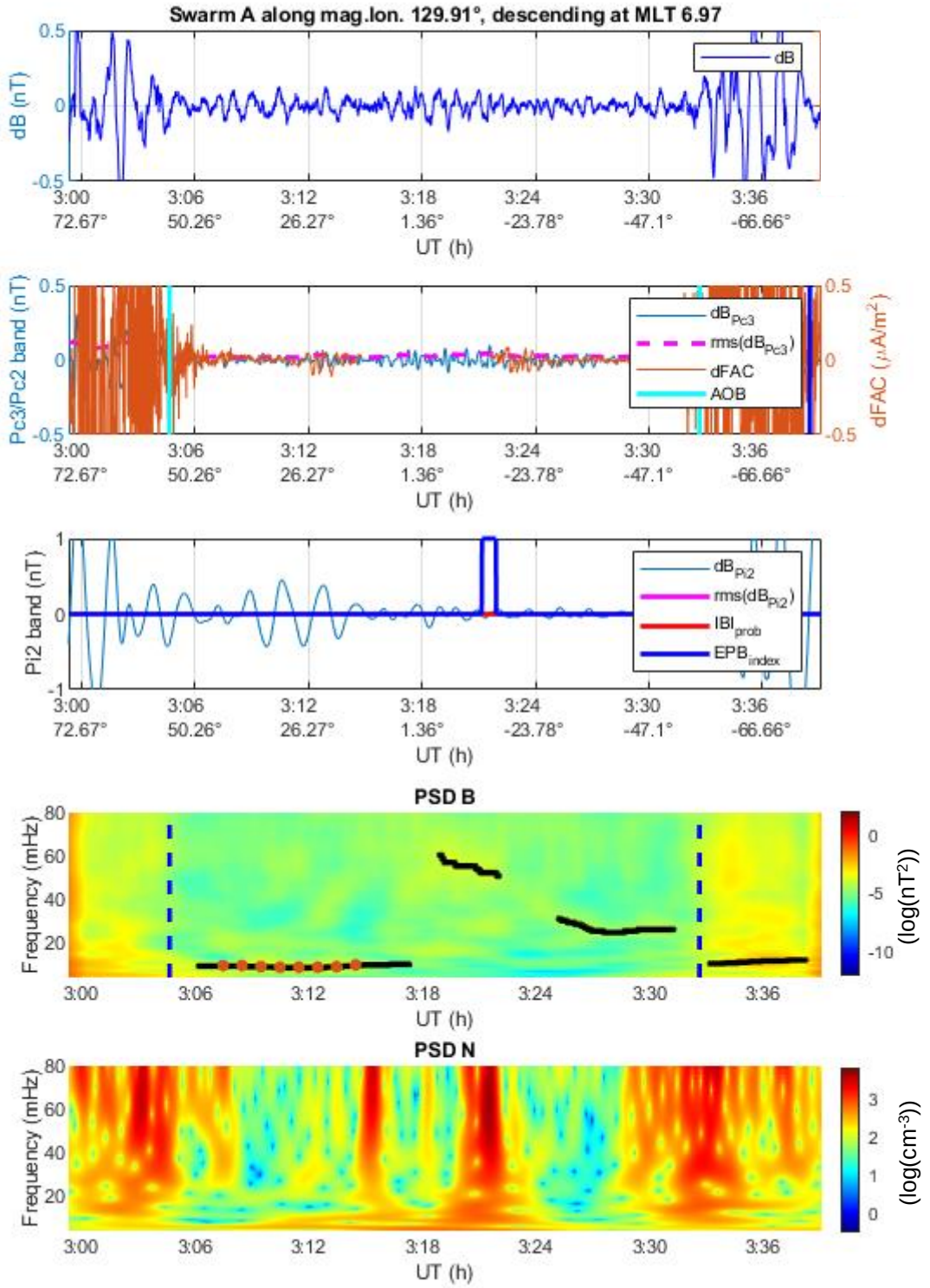


Figure 2, A visualisation example of the ULF wave product parameters (Swarm A, March 18, 2015 03:00-03:38 UT, MLT = 07). (1st) high-pass (f_c at 12 mHz) filtered $\boldsymbol{dB_p}$, (2nd) $\boldsymbol{dB_p}$ filtered in the Pc3 band (blue), Pc3 act(ivity) (dashed magenta), FAC (red), AOB (vertical cyan), (3rd) $\boldsymbol{dB_p}$ filtered in the Pi2 band (light blue), flag_EPB (blue), IBI index (red), (4th) wavelet spectrogram of $\boldsymbol{dB_p}$ (background), detected potential wave events (black), dominant frequency (red dots), and plasmapause location proxy (dashed blue), (5th) wavelet spectrogram of electron density fluctuations.

The use and/or disclosure, etc. of the contents of this document (or any part thereof) is subject to the restrictions referenced on the front page.

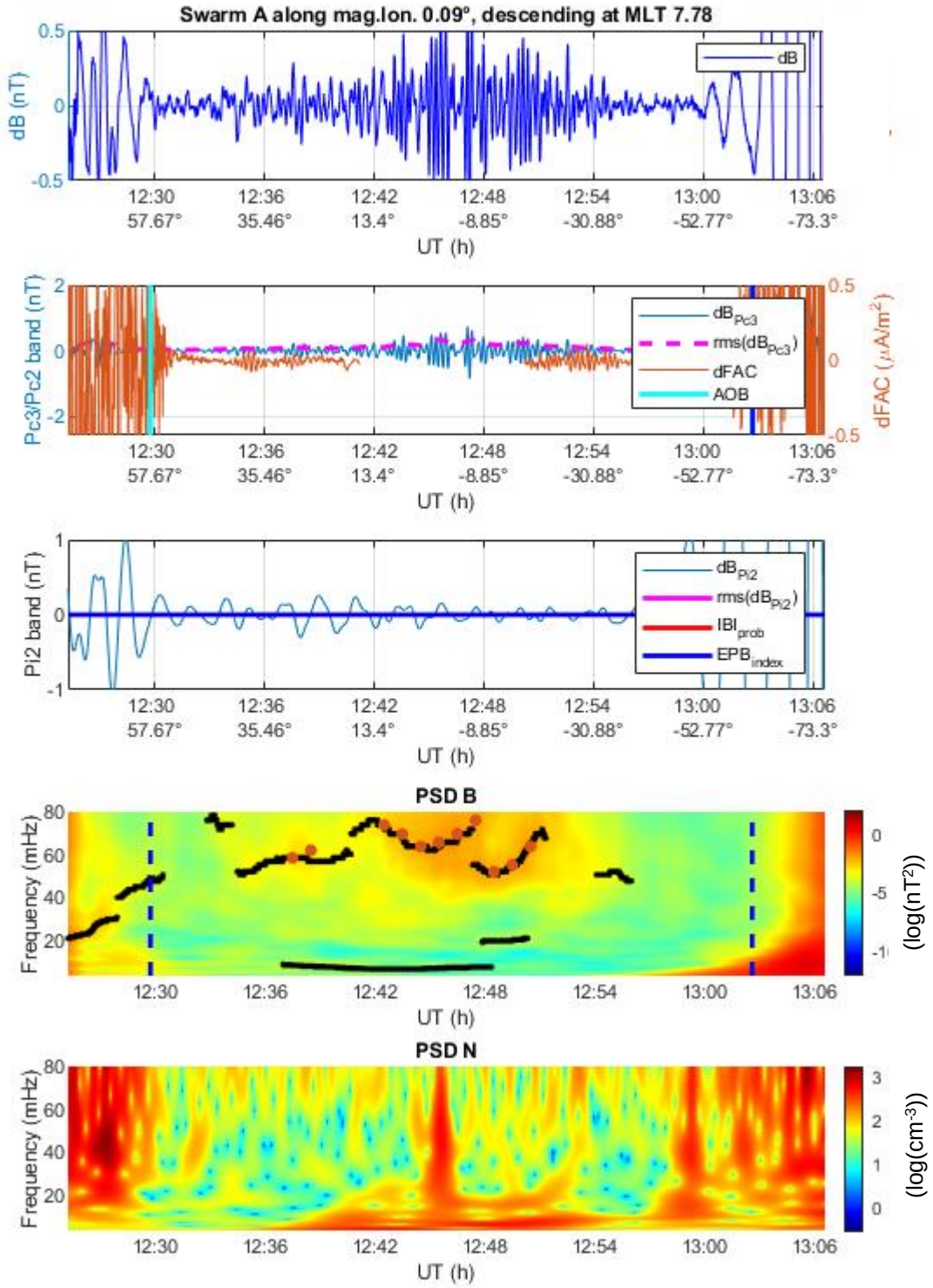


Figure 3, Same as Figure 2 but for 12:27-13:06 UT, MLT = 7.8.

The use and/or disclosure, etc. of the contents of this document (or any part thereof) is subject to the restrictions referenced on the front page.

4.1.3.4 *Calculation of one-minute means of position and time*

Finally, the one-minute mean of the geographic and geomagnetic coordinates, UT and MLT, and SZA are calculated.

4.1.3.5 *Flag definitions*

Several flags are defined in the context of one-minute activity indices to identify various features in the data.

Flag_FAC is an indicator of FAC intensity:

Flag_FAC := 0, if FAC_act <= .05 $\mu A/m^2$

Flag_FAC := 1, if 0.05 $\mu A/m^2$< FAC_act <= 0.1 $\mu A/m^2$,

Flag_FAC := 2, if 0.1 $\mu A/m^2$ < FAC_act <= 0.2 $\mu A/m^2$,

Flag_FAC := 3, if 0.2 $\mu A/m^2$ < FAC_act <= 0.5 $\mu A/m^2$,

Flag_FAC := 4, if 0.5 $\mu A/m^2$ < FAC_act.

Flag_EPB is an indicator of Equatorial Plasma Bubbles. It is derived based on the phase difference (from cross-wavelet spectra) between the time-differentiated compressional magnetic field (ddB_p) and the similarly time-differentiated density (dNe) fluctuations. The phase difference is calculated only when the coherence is above 0.5. The maximum phase difference between the two signals is calculated over the 25-80 mHz frequency band and for each minute. Whenever the maximum phase difference at low latitude (QD latitude < 25°) is above 120° (i.e. when the density and the compressional fluctuations are in anti-phase) and the band (25-80 mHz) averaged density fluctuations surpass a certain threshold ($\log_{10}$ (|CWT(dNe)|) = 3.2), this flag is set to 1, indicating the likely presence of plasma bubbles. This value corresponds to a ~1600 cm^{-3} amplitude density fluctuation and is based on our experience.

Flag_EPB: = 1, if max(unwrap(angle(CWT(dNe))-angle(CWT($ddB_{p,Pxn}$))) > 120° and ($\log_{10}$(|CWT(dNe)|) > 3.2 and |QD latitude| Is < 25°,

otherwise, Flag_EPB = 0.

Flag_Pc2 is an indicator of likely Pc2 wave activity defined as:

Flag_Pc2 = 1 if Pc2_act > 12 pT and Flag_FAC == 0 and Flag_EPB == 0,

Flag_Pc2 = 2 if Pc2_act > 12 pT and Flag_FAC == 0 and Flag_EPB == 0 and two closeby satellites are in phase,

otherwise, Flag_Pc2 = 0.

Thus Flag_Pc2 = 1 when there is no indication of intense FACs or EPBs and the Pc2 activity surpasses a certain level. Similarly

Flag_Pc3 is an indicator of likely Pc3 wave activity defined as:

Flag_Pc3 = 1 if Pc3_act > 20 pT and Flag_FAC == 0 and Flag_EPB == 0,

Flag_Pc3 = 2 if Pc3_act > 20 pT and Flag_FAC == 0 and Flag_EPB == 0 and two closeby satellites are in phase,

otherwise, Flag_Pc3 = 0.

Flag_Pc4 is an indicator of likely Pc4 wave activity defined as:

The use and/or disclosure, etc. of the contents of this document (or any part thereof) is subject to the restrictions referenced on the front page.

Flag_Pc4 = 1 if Pc4_act > 20 pT and Flag_FAC == 0 and Flag_EPB == 0,

Flag_Pc4 = 2 if Pc3_act > 20 pT and Flag_FAC == 0 and Flag_EPB == 0 and two closeby satellites are in phase,

otherwise, Flag_Pc4= 0.

Flag_Pi2 is an indicator of likely Pi2 wave activity defined as:

Flag_Pi2 = 1 if Pi2_act > 20 pT and Flag_FAC == 0 and Flag_EPB == 0,

Flag_Pi2 = 2 if Pi2_act > 20 pT and Flag_FAC == 0 and Flag_EPB == 0 and two closeby satellites are in phase,

otherwise, Flag_Pi2 = 0.

Whether the wave observations of two close-by (latitude and longitude separation is less than 30°) satellite are in phase is judged from the median phase difference of the coherent frequency components in the considered Pc2, Pc3, Pc4 or Pi2 frequency bands. The delay time calculated from the wave observations is compared to the follow time between two satellites. The latter is always kept above 4 s (except for a few weeks in 2022). Whenever the delay time calculated from wave observations is below 2 s, the two events are considered to be in-phase.

4.1.3.6 *Product variables*

Variable Name	Type	Dimension	Temporal resolution	Unit	Description
Timestamp	CDF_EPOCH	1	1 min	-	Time of observation, UTC
Latitude	CDF_DOUBLE	1	1 min	deg	Position in ITRF – Geocentric latitude
Longitude	CDF_DOUBLE	1	1 min	deg	Position in ITRF – Geocentric longitude
Radius	CDF_DOUBLE	1	1 min	m	Position in ITRF – Geocentric radius
Latitude_QD	CDF_DOUBLE	1	1 min	deg	Quasi-Dipole latitude
Longitude_QD	CDF_DOUBLE	1	1 min	deg	Quasi-Dipole longitude
UT	CDF_DOUBLE	1	1 min	hr	Universal Time
MLT	CDF_DOUBLE	1	1 min	hr	Magnetic Local Time
SZA	CDF_DOUBLE	1	1 min	deg	Solar zenith angle
Frequency_dominant	CDF_DOUBLE	1	1 min	mHz	Dominant frequency
Halfwidth	CDF_DOUBLE	1	1 min	mHz	Spectral peak half width
Power	CDF_DOUBLE	1	1 min	$\log(nT^2)$	Peak signal power
Prominence	CDF_DOUBLE	1	1 min	-	Peak prominence

The use and/or disclosure, etc. of the contents of this document (or any part thereof) is subject to the restrictions referenced on the front page.

Variable Name	Type	Dimension	Temporal resolution	Unit	Description
Pc2_act	CDF_DOUBLE	1	1 min	pT	Rms of the fluctuations in the Pc2 band
Pc3_act	CDF_DOUBLE	1	1 min	pT	Rms of the fluctuations in the Pc3 band
Pc4_act	CDF_DOUBLE	1	1 min	pT	Rms of the fluctuations in the Pc4 band
Pi2_act	CDF_DOUBLE	1	1 min	pT	Rms of the fluctuations in the Pi2 band
Flag_Pc2	CDF_UINT1	1	1 min	-	Flag indicating the presence of Pc2 waves (see Section 4.1.3.5 for further details)
Flag_Pc3	CDF_UINT1	1	1 min	-	Flag indicating the presence of Pc3 waves (see Section 4.1.3.5 for further details)
Flag_Pc4	CDF_UINT1	1	1 min	-	Flag indicating the presence of Pc4 waves (see Section 4.1.3.5 for further details)
Flag_Pi2	CDF_UINT1	1	1 min	-	Flag indicating the presence of Pi2 waves (see Section 4.1.3.5 for further details)
Flag_FAC	CDF_UINT1	1	1 min	-	Flag indicating intense FAC activity (see Section 4.1.3.5 for further details)
Flag_EPB	CDF_UINT1	1	1 min	-	Flag indicating significant EPB activity (see Section 4.1.3.5 for further details)

4.1.4 Main steps of the detection process

4.1.4.1 *Segmentation of the data into quarter of half orbits*

The detection process is carried out along a pole-to-pole profile. Based on the magnetic coordinates, all full Swarm orbits are divided into two pole-to-pole segments. The segments are identified in the data files by the orbit number (taken from AUXxORBCNT product) and the direction of flight (+1/-1 for ascending/descending, respectively.

The use and/or disclosure, etc. of the contents of this document (or any part thereof) is subject to the restrictions referenced on the front page.

4.1.4.2 *Analysis of a pole-to-pole profile – calculation of spectra, coherence and phase difference*

The continuous wavelet spectra (Morlet as mother wavelet) are calculated for the time-differentiated compressional field component, also for the time-differentiated density fluctuations. The frequency scale applied for spectral calculations is 24 frequencies per octave, ranging from 4 mHz to 128 mHz. The further processing was based on the logarithm of the power spectra, i.e.:

$$D = 2 \cdot \log_{10}(|CWT(dNe)|),$$

$$S = 2 \cdot \log_{10}(|CWT(dB_p)|).$$

Before the spectral analysis, *S* is smoothed along its time dimension using a 120 s long running window:

$$S_{sm}(t) = \frac{1}{120} \sum_{\tau=t-60}^{\tau=t+59} S(\tau).$$

Moreover, the phase difference spectra between these two signals, as well as between satellite 1 and 2 (A and C or C and A) were also calculated. The phase difference spectra (phase difference as a function of frequency and time) were derived from the wavelet spectra but only at frequencies where the coherence is greater than 0.75. Otherwise, the phase difference was set to NaN to exclude from further calculation.

$$xPH_{BN} = \text{angle}(CWT(dNe)) - \text{angle}\left(CWT(dB_p)\right),$$

$$xPH_{BN}(\text{COH}(dNe, dB_p) < 0.75) = \text{NaN}.$$

$$xPH_{B1,B2} = \text{angle}\left(CWT(dB_{p2})\right) - \text{angle}\left(CWT(dB_{p1})\right),$$

$$xPH_{B1B2}(\text{COH}(dB_{p1}, dB_{p2}) < 0.75) = \text{NaN}.$$

These phase difference spectra are used to derive Flag_EPB and Flag_AC as mentioned briefly in Section 4.1.3.5.

4.1.4.3 *Wave event detection*

The event detection starts with the detection of all significant spectral peak in the pole-to-pole spectra. The significance criteria applied are:

1) the amplitude is greater than a given threshold ($S_{sm} > -5$), and
2) the peak prominence is greater than $\Delta S_{sm} > 0.6$ (at least twice the background).

Although the threshold for S_{sm} is the same for all frequencies, since it is applied on time-differentiated spectra, in fact it represents a frequency-dependent threshold which is around 25/10/5 pT for 20/50/100 mHz, respectively (see Figure 4). Once the peaks are identified, their power are corrected for the decrease introduced by the time differentiation (while prominences are left as they are).

The use and/or disclosure, etc. of the contents of this document (or any part thereof) is subject to the restrictions referenced on the front page.

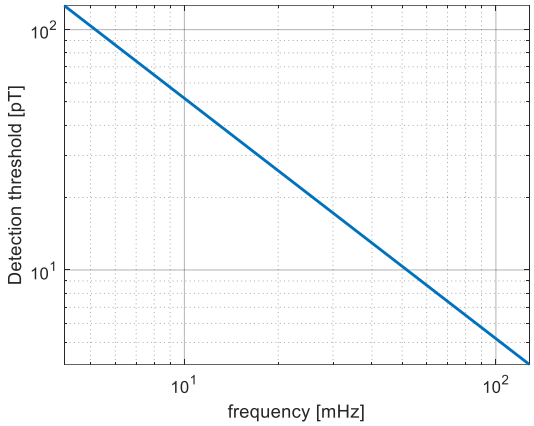


Figure 4, Peak detection threshold as a function of frequency

The prominence, power and half width associated with the detected peaks are also stored, as well as spatial, temporal coordinates, the solar zenith angle, the plasma bubble indicator, and the rms FAC intensity calculated from 60s of FAC data, as potential wave event characteristics.

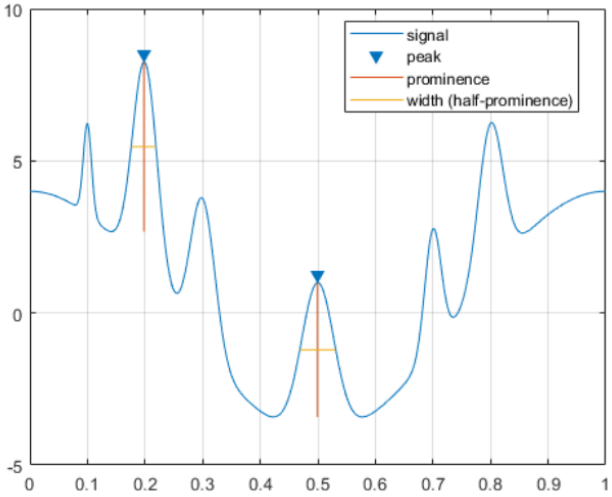


Figure 5, Half width (called width in this figure) is defined at half of the peak prominence (an artificial example curve composed of a full period cosine and six Gaussian).

As a result of this initial detection step, one may get from zero to several peaks for each second (column of the spectrum). All the peaks detected in the spectrum are then grouped into connected sets. The process starts with taking at one of the earliest in time (t_1) peaks and then looking for its closest neighbour at t_i+1. A peak is accepted as a neighbour if its distance in time and frequency is less than or equal to 3 s and 3 spectral line, respectively. If such a point is found, it is added to the first set. If no such a neighbour is found, the next one of the earliest in time (t_j) peaks is taken (i can be equal to j), as the first element of a new set. This grouping process continues until all the spectral peaks have been ordered into these interconnected sets.

In the next steps, all the sets shorter than three times the wave period are sorted out. This criterion is frequency dependent, the period is calculated from the frequency observed with the greatest power. Sets with maximum prominence less than 1.2 (amplitude 4x the background) are also sorted out. The sets surviving this step are called events.

An event is identified by the triplet of the orbit number (ORB_e), the flight direction (DIR_e) and the event serial number (ID_e). Note, that ID_e is assigned to the event in the step when the connected sets are

The use and/or disclosure, etc. of the contents of this document (or any part thereof) is subject to the restrictions referenced on the front page.

compiled. At later steps, some of the sets (and their ID_e) are removed, and the sets are reordered. As a consequence, ID_e is not an increasing sequence of consecutive numbers.

Quality_e provides instantaneous quality information derived from instantaneous spectral properties, as well as from signatures of possible contaminations of wave observations by FACs or EPB phenomena. Definition of the flag values is as follows:

3: if EPB_e = 0 AND FAC_e < 0.2 $\mu A/m^2$ (no contamination from plasma bubbles; FAC intensity is very low)

2: if EPB_e = 0 AND 0.2 $\mu A/m^2$ ≤ FAC_e < 0.5 $\mu A/m^2$ (no contamination from plasma bubbles; low FAC intensity)

-1: if 0.5 $\mu A/m^2$ ≤ FAC_e OR EPB_e = 1 (no contamination from plasma bubbles; FAC intensity is from medium to high OR plasma bubble contamination is likely present)

0: if no information is available on EPB.

4.1.4.4 *Product variables*

Variable Name	Type	Dimension	Temporal resolution	Unit	Description
ORB_e	CDF_UINT4	1	1 s	-	Orbit number for ID event points (where ID is the Event identifier ID_e, see below)
DIR_e	CDF_INT1	1	1 s	-	Flight direction for ID event points (1: ascending, -1: descending)
ID_e	CDF_UINT1	1	1 s	-	Event identifier (a serial unique for the event)
Timestamp_e	CDF_EPOCH	1	1 s	ms	Time of observation for ID event points, UTC
Latitude_e	CDF_DOUBLE	1	1 s	deg	Position in ITRF – Geocentric latitude for ID event points
Longitude_e	CDF_DOUBLE	1	1 s	deg	Position in ITRF – Geocentric longitude for ID event points
Radius_e	CDF_DOUBLE	1	1 s	m	Position in ITRF – Geocentric radius for ID event points
Latitude_QD_e	CDF_DOUBLE	1	1 s	deg	Quasi-dipole latitude for ID event points
Longitude_QD_e	CDF_DOUBLE	1	1 s	deg	Quasi-dipole longitude for ID event points
MLT_e	CDF_DOUBLE	1	1 s	hr	Magnetic Local Time for ID event points
SZA_e	CDF_DOUBLE	1	1 s	deg	Solar zenith angle for ID event points

The use and/or disclosure, etc. of the contents of this document (or any part thereof) is subject to the restrictions referenced on the front page.

Variable Name	Type	Dimension	Temporal resolution	Unit	Description
Frequency_e	CDF_DOUBLE	1	1 s	mHz	Instantaneous frequency for ID event points
Halfwidth_e	CDF_DOUBLE	1	1 s	mHz	Instantaneous spectral peak half width for ID event points
Power_e	CDF_DOUBLE	1	1 s	$\log(nT^2)$	Instantaneous peak power for ID event points
Prominence_e	CDF_DOUBLE	1	1 s	-	Instantaneous peak prominence for ID event points
EPB_e	CDF_INT1	1	1 s	-	Instantaneous plasma bubble indicator for ID event points
FAC_e	CDF_DOUBLE	1	1 s	$\mu A/m^2$	Instantaneous rms FAC intensity for
Flag_B_e	CDF_UNIT1	1	1 s	-	Instantaneous Flag_B from MAGx_LR L1b product
Quality_e	CDF_INT1	1	1 s	-	Instantaneous Quality for ID event for ID event points (see Section 4.1.4.3)

4.1.4.5 *Calculation of event mean properties*

The event mean characteristics, such as event duration, mean frequency and standard deviation of the frequency, prominence, power and half width of the peak, along with spatial and temporal coordinates are calculated for each event.

The overall event quality Quality_m is derived as the median of Quality_e values for the considered event. However, if the maximum prominence of the events stays below 1.8, Quality_m is decreased by one (from 3 to 2 or from 2 to 1).

4.1.4.6 *Product variables*

Variable Name	Type	Dimension	Temporal resolution	Unit	Description
ORB_m	CDF_UINT4	1	per event	-	Orbit number for event mean properties
DIR_m	CDF_INT1	1	per event	-	Flight direction for event mean properties

The use and/or disclosure, etc. of the contents of this document (or any part thereof) is subject to the restrictions referenced on the front page.

Variable Name	Type	Dimension	Temporal resolution	Unit	Description
ID_m	CDF_UINT1	1	per event	-	Event identifier for event mean properties
Timestamp_m	CDF_EPOCH	1	per event	ms	Event mean time of observation, UTC
Latitude_m	CDF_DOUBLE	1	per event	deg	Event mean position in ITRF – Geocentric latitude
Longitude_m	CDF_DOUBLE	1	per event	deg	Event mean position in ITRF – Geocentric longitude
Radius_m	CDF_DOUBLE	1	per event	m	Event mean position in ITRF – Geocentric radius
Latitude_QD_m	CDF_DOUBLE	1	per event	deg	Event mean quasi-dipole latitude
Longitude_QD_m	CDF_DOUBLE	1	per event	deg	Event mean quasi-dipole longitude
MLT_m	CDF_DOUBLE	1	per event	hr	Event mean Magnetic Local Time
SZA_m	CDF_DOUBLE	1	per event	deg	Event mean solar zenith angle
Duration_m	CDF_DOUBLE	1	per event	min	Event duration
Frequency_m	CDF_DOUBLE	1	per event	mHz	Event mean ULF frequency
Freq_std_m	CDF_DOUBLE	1	per event	mHz	Standard deviation of the spectral peak
Halfwidth_m	CDF_DOUBLE	1	per event	mHz	Event mean spectral peak half-width
Power_m	CDF_DOUBLE	1	per event	$\log(nT^2)$	Event mean power
Prominence_m	CDF_DOUBLE	1	per event	-	Event mean prominence
EPB_m	CDF_INT1	1	per event	-	Event peak plasma bubble indicator
FAC_m	CDF_DOUBLE	1	per event	$\mu A/m^2$	Event peak rms FAC intensity
Flag_B_m	CDF_UINT1	1	per event	-	Event maximum Flag_B from MAGx_LR L1b product
Quality_m	CDF_INT1	1	per event	-	Overall event quality (see Section 4.1.4.)

The use and/or disclosure, etc. of the contents of this document (or any part thereof) is subject to the restrictions referenced on the front page.

4.1.4.7 *Saving the data in daily cdf product files*

Finally, all the product variables are written into daily cdf files. The name of the cdf files follow the Swarm convention [AD-4]. The file name has the format:

MM_CCCC_FFFxDDD_2z_yyyymmddThhmmss_YYYYMMDDTHHMMSS_vvvv.EXT,

where 'MM' stands for the mission identifier ('SW' for Swarm), 'CCCC' is the type of the product (here 'OPER' for operational), 'FFFxDDD_2z' is the product name, 'yyyymmddThhmmss' and 'YYYYMMDDTHHMMSS' are the validity start and stop time (i.e., the time of the first and last data record in the file that is 00:00:00 and 23:59:59 for daily files), respectively, while 'vvvv' is the version number. For this product 'EXT' is always 'cdf'. The product name consists of the following elements: 'ULF' ('FFF') to identify the target of the product, followed by the identifier of the Swarm satellite ('A', 'B' or 'C'), 'DDD' is 'MAG' referring to the source data identifier, finally '2F' is used for '2z', indicating that this is a Level-2 Fast Track product. An example is given below:

SW_OPER_ULFAMAG_2F_20150402T000000_20150402T235959_0101.cdf

The content of the file is detailed in [AD-2], however, the variables are also listed in this document in Sections 4.1.3.6, 4.1.4.4, and 4.1.4.6.

Note that product files are only generated when the input MAGx_LR file for the day considered is complete, i.e. starts and ends at midnight. Although short gaps are filled, longer gaps could easily lead to contaminated filtered signals and false detections or characterisation. Whenever a complete MAGx_LR input file is available, the ULFxMAG product is generated. Missing EFI and FAC files only affect the calculation of some flags. Flags are zero when for any reason the relevant information is not available.

4.2 Pc1 wave detection

The automatic detection and characterization of Pc1 geomagnetic pulsations based on HR magnetometer data (MAGx_HR_1B) consists of five main steps (see also Figure 6 presenting the process in a flowchart). First, the magnetic measurements are transformed into a field-aligned coordinate system. Then, the spectrograms of the field components are calculated, and different types of noise are removed from the spectrograms. In the third step, Pc1 candidate events are determined based on peak finding and the coherence of the field components. Next, the spectral peaks are grouped into events. Finally, the mean properties of the identified Pc1 events are calculated. These main steps are described in detail in the following subsections.

4.2.1 Reading the data

Input high-frequency magnetic data (MAGx_HR L1b product in NEC frame) for the day considered are read from the source cdf file. The daily data are complemented by the last segment fragment (from the last magnetic pole crossing) of the previous day so that the daily data contains complete pole-to-pole orbits. At the same time, the last orbit fragment is dropped since it is to be analysed together with data from the following day. The orbit counter is read from the AUXxORBCNT product files.

The use and/or disclosure, etc. of the contents of this document (or any part thereof) is subject to the restrictions referenced on the front page.

4.2.2 Pre-processing

4.2.2.1 *Calculation of auxiliary data*

The calculation of quasi-dipole coordinates, the L-values (L=1⁄(cos^2 ϕ), where ϕ is the QD-latitude), magnetic local time (MLT) and solar zenith angle (SZA) is done for all data points separately. The applied routines are the *qdipole* routine (written and maintained by N. Olsen, DTU) and the *solar_zenith_angle* routine (by P. Ritter, GFZ and N. Olsen, DTU).

The use and/or disclosure, etc. of the contents of this document (or any part thereof) is subject to the restrictions referenced on the front page.

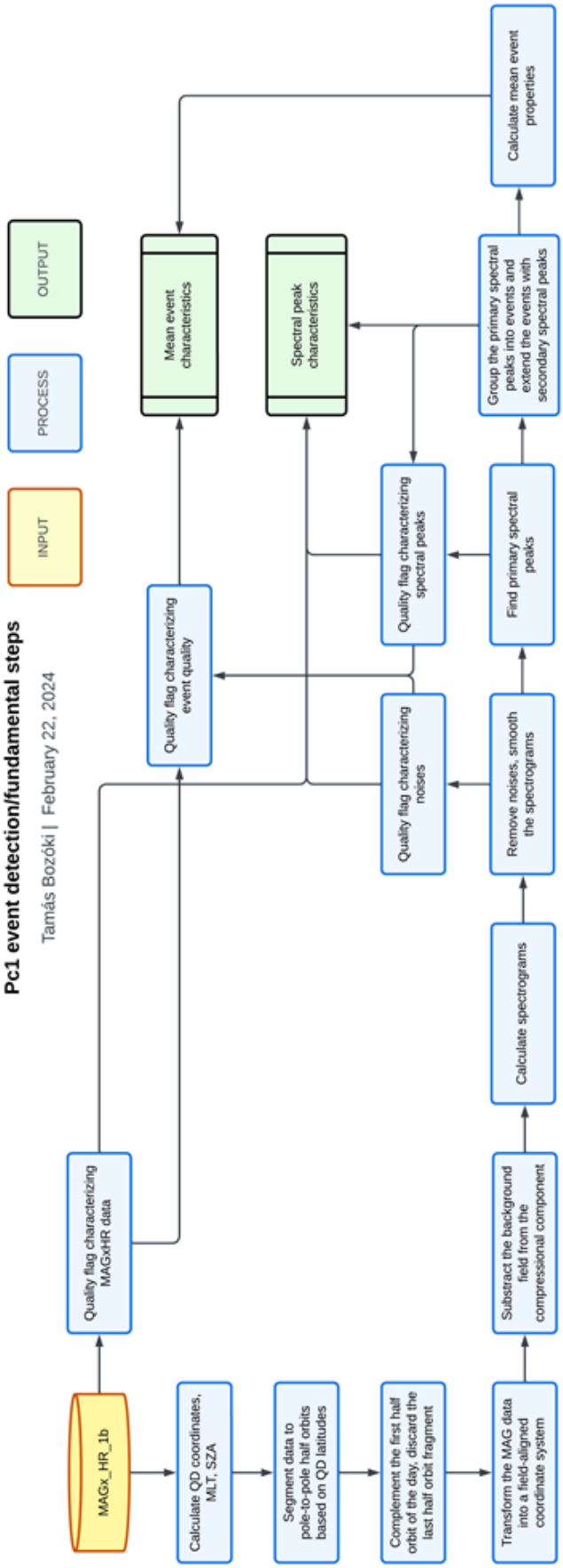


Figure 6, Flowchart showing the main steps of Pc1 event detection

The use and/or disclosure, etc. of the contents of this document (or any part thereof) is subject to the restrictions referenced on the front page.

4.2.2.2 *Segmentation of the data into half orbits*

All the data is segmented into (magnetic) pole-to-pole half-orbits and all subsequent processing steps are performed segment by segment. The first half-orbit of the day is completed with the end of the previous day, while the end of the last, incomplete half-orbit of the given day is processed together with the next day. The magnetic poles are found based on the extrema of the down-sampled magnetic latitude records. The half-orbit segments are described by the official Swarm orbit counts and whether they are ascending or descending half-orbits (based on the ORBCNT Level 1b data product).

4.2.2.3 *Transforming the high-frequency magnetic measurements into a field-aligned coordinate system*

The background magnetic field is determined using a Savitzky-Golay filter with a 30-second moving window (30×50+1 data points) and a polynomial degree of 2 [RD-17]. The original measurements are transformed into a field-aligned coordinate system in which the *p*-axis is parallel to the background magnetic field, the *a*-axis (azimuthal) is perpendicular to the plane formed by the *p*-axis and the centre of the Earth, pointing to the East, while the *r*-axis (radial) completes the right-hand triad. Thus, the B_p component will include the compressional Pc1 events, while the B_a/B_r components the transversal Pc1 events.

4.2.2.4 *Removal of the mean field*

The background magnetic field is subtracted from the new magnetic B_p component to obtain the fluctuation field in this field component as well (since the other two field components are perpendicular to the background magnetic field, they represent the fluctuation field immediately after the coordinate transformation).

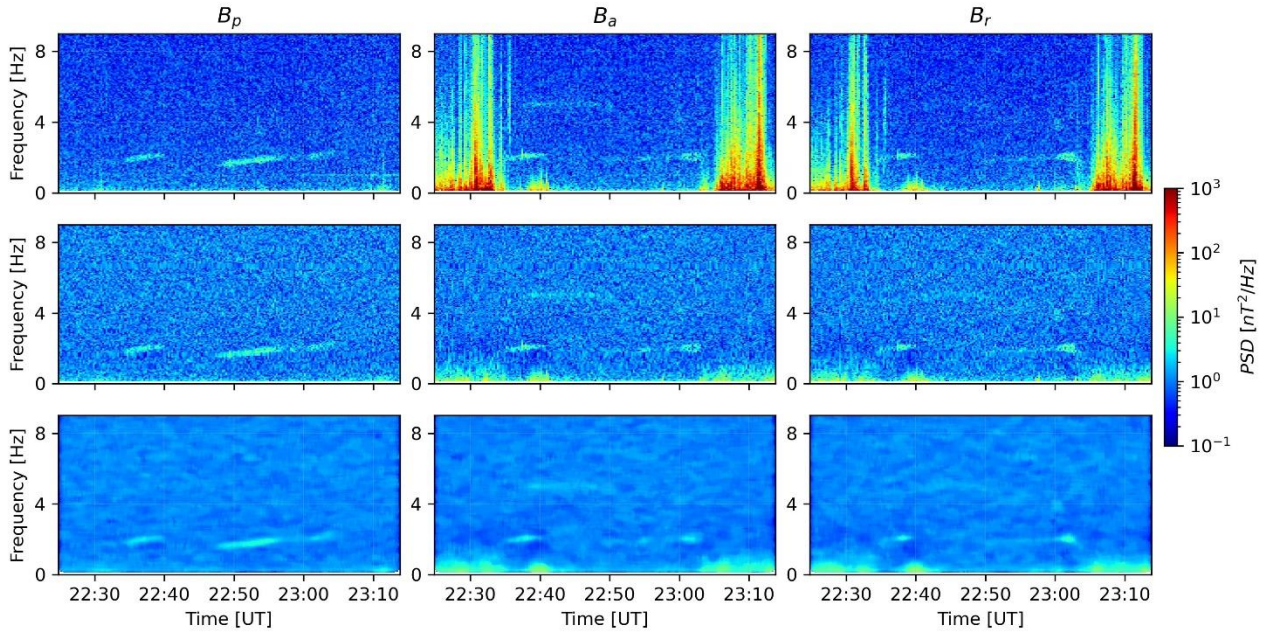


Figure 7 A visualisation example of the noise removal procedure for the 30th half orbit on 18 March, 2015. The first, second and third columns show the spectrograms of the $\boldsymbol{B_p}$, $\boldsymbol{B_a}$ and $\boldsymbol{B_r}$ components of the fluctuation magnetic field, respectively. The top, middle and bottom rows correspond to the original, raw spectrograms (top), to the spectrograms from where 1/f type and narrowband noises had been removed (middle), and to the final, smoothed spectrograms. See the text for more details.

The use and/or disclosure, etc. of the contents of this document (or any part thereof) is subject to the restrictions referenced on the front page.

4.2.3 Main steps of the detection process

4.2.3.1 *Determining spectrograms and noise removal*

The power spectral density (PSD) spectrograms of the 50 Hz magnetic field components are determined using a 1024-point window length, 273-point overlap and the Hamming function for windowing [RD-17]. Frequencies below 0.1 Hz and above 9.5 Hz are removed from the spectrograms (resulting in 191 data points along the frequency axis). 1/f type noise is removed from each spectrum by subtracting a smooth back-ground spectrum obtained by a moving average of 81 points (~4 Hz) in the logarithm of the data. If the number of data points exceeding 1 nT^2/Hz is greater than 64, then the spectrum is likely to be contaminated by local field aligned currents [RD-17]. This information is indicated by a data quality flag in the final data product. In the spectrograms of Swarm high-frequency magnetic data, narrowband noises of artificial origin occur sometimes at the following frequencies: 1 Hz, 1.5 Hz, 1.66 Hz, 2 Hz, 3 Hz, 5 Hz, and 6.66 Hz. These narrowband noises are removed from the spectrograms by replacing them with the average spectral intensity values of the adjacent frequencies. Next, a two-dimensional (7×7) median filter is applied to eliminate sharp stand-alone peaks from the spectrograms. As an example of the application of this noise removal procedure see Figure 7. Information on the satellite position (latitude, longitude, radius, magnetic latitude, magnetic longitude, MLT, SZA) are resampled for the time instants of the spectrograms.

4.2.3.2 *Pc1 candidate event search based on peak finding and coherence*

The determination of Pc1 candidate events is based on the built-in Matlab function *findpeak*, which is run with empirically determined peak criteria (minimum peak prominence: 1.5 nT^2/Hz, minimum peak width: 0.15 Hz, minimum peak distance: 0.15 Hz) on each spectrum of the spectrograms. If the algorithm finds a peak in one of the magnetic field components, it is tested whether the same peak is found in the other two field components based on a coherence criterion (the cross-coherence needs to be higher than 0.7). If the coherence criterion is not met, the prominence of the peak must fulfil a stronger peak prominence criterion (2.0 nT^2/Hz). To determine the width of the peaks, the smoothed derivative spectrum is used, with the nearest values below 0.08 around the given peak defining the upper and lower widths (unless the *findpeak* function returns a larger width value).

4.2.3.3 *Identifying and extracting individual Pc1 events*

In this step, the previously identified spectral peaks are grouped according to whether they belong to the same Pc1 event based on their temporal and frequency proximity. These individual Pc1 events are then extended in time, using a less strict peak criterion than in the original case. If two events are less than 30 seconds apart in time and their peak frequencies are close to each other (i.e., within the peak widths), they are merged into one event. In this case, the missing spectral peak values in the gap between the two events are determined by interpolation (hence all events are continuous in time). The peak locations and widths of the events are smoothed by applying a second-order polynomial fit, weighted according to whether the actual peak was found by the primary peak search (hereinafter referred to as primary spectral peaks) or was appended to the event only during the event extension (hereinafter referred to as secondary spectral peaks). All events determined by this procedure need to be at least 1 minute in duration to be considered as real events.

The use and/or disclosure, etc. of the contents of this document (or any part thereof) is subject to the restrictions referenced on the front page.

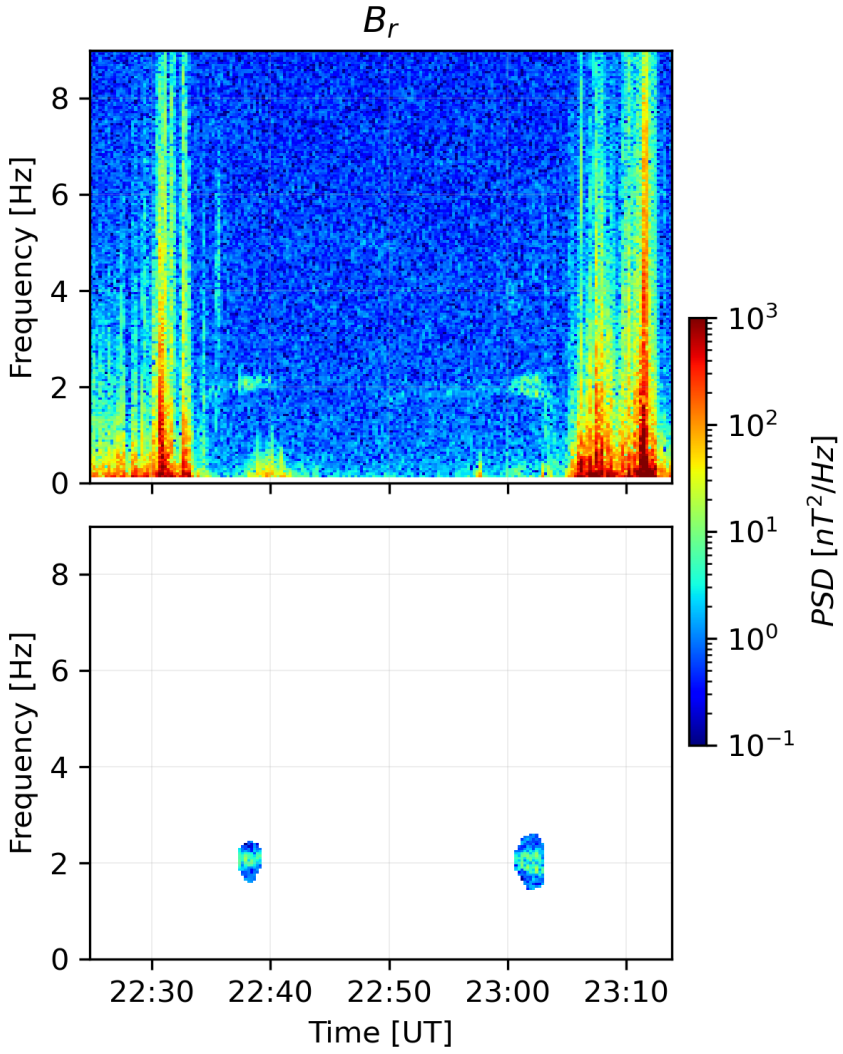


Figure 8, A visualisation example of events identified in the B_r component for the 30th half orbit on 18 March, 2015. The top figure shows the original, raw spectrogram, while the bottom figure shows those areas of the spectrogram that correspond to the identified two Pc1 events.

4.2.3.4 *Quality flags characterizing spectral peaks*

Three different quality flags are introduced (Quality_B, Quality_p, Quality_n) for characterizing the quality of the spectral peaks.

Quality_B contains (interpolated) Flag_B values from the MAGx_HR data files (see the documentation of MAGx_HR for more details).

Quality_p indicates whether the data point corresponds to a primary (1) or a secondary (2) spectral peak (see section 4.2.3.2).

Quality_n indicates whether strong 1/f type noise (likely related to field-aligned currents) was present in the original spectrum (see section 4.2.3.1). 0 stands for noise free spectra and 1 for spectra with strong 1/f type noise.

4.2.3.5 *Product variables characterizing spectral peaks*

All the spectral peaks identified in the process described above are characterised by the product variables summarised in the following table:

The use and/or disclosure, etc. of the contents of this document (or any part thereof) is subject to the restrictions referenced on the front page.

Variable Name	Type	Dim	Unit	Description
ORB_C	CDF_UINT2	1	-	Orbit number for the Bp/Ba/Br component ID event (where ID is the event identifier ID_C, see below), and C stands for any of the three components
DIR_C	CDF_INT1	1	-	Flight direction for the Bp/Ba/Br component ID event (1: ascending, -1: descending)
ID_C	CDF_UINT1	1	-	Bp/Ba/Br component event identifier
Timestamp_C	CDF_EPOCH	1	-	Time of observation for the Bp/Ba/Br component ID event, UTC
Latitude_C	CDF_DOUBLE	1	deg	Position in ITRF – Geocentric latitude for the Bp/Ba/Br component ID event
Longitude_C	CDF_DOUBLE	1	deg	Position in ITRF – Geocentric longitude for the Bp/Ba/Br component ID event
Radius_C	CDF_DOUBLE	1	m	Position in ITRF – Geocentric radius (from the Earth centre) for the Bp/Ba/Br component ID event
Latitude_QD_C	CDF_DOUBLE	1	deg	QD latitude for the Bp/Ba/Br component ID event
Longitude_QD_C	CDF_DOUBLE	1	deg	QD longitude for the Bp/Ba/Br component ID event
MLT_C	CDF_DOUBLE	1	hr	Magnetic Local Time for the Bp/Ba/Br component ID event
SZA_C	CDF_DOUBLE	1	deg	Solar zenith angle for the Bp/Ba/Br component ID event
Frequency_C	CDF_DOUBLE	1	Hz	Instantaneous frequency for the Bp/Ba/Br component ID event
Halfwidth_C	CDF_DOUBLE	1	Hz	Instantaneous spectral peak half width for the Bp/Ba/Br component ID event

The use and/or disclosure, etc. of the contents of this document (or any part thereof) is subject to the restrictions referenced on the front page.

Variable Name	Type	Dim	Unit	Description
Power_C	CDF_DOUBLE	1	nT^2/Hz	Instantaneous power for the Bp/Ba/Br component ID event
Prominence_C	CDF_DOUBLE	1	-	Instantaneous prominence for the Bp/Ba/Br component ID event
Quality_B_C	CDF_UINT1	1	-	Instantaneous MAGxHR quality for the Bp/Ba/Br component ID event. = Flag_B of the MAGx_HR product, see the documentation of MAGx_HR for details.
Quality_p_C	CDF_UINT1	1	-	Instantaneous peak quality for the Bp/Ba/Br component ID event. 1: primary spectral peak, 2: secondary spectral peak (see [AD-2] for further details)
Quality_n_C	CDF_UINT1	1	-	Instantaneous noise quality for the Bp/Ba/Br component ID event. 0: 1/f type noise not present, 1: 1/f type noise present (see [AD-2] for further details)

4.2.3.6 *Quality flag characterizing individual Pc1 events*

From the three different quality flags introduced to characterise spectral peaks, one single quality flag is determined to characterise each Pc1 event. The values of the quality flag are integers ranging from 0 to 7, with the following meaning:

0: high quality data

1: not nominal operation of the VFM instrument*

2: low number of primary data points**

3: contaminated spectra***

4: 1 and 2

5: 1 and 3

6: 2 and 3

7: 1 and 2 and 3

*if the modus of Quality_B of the spectral peaks is not 0.

**if the relative number of Quality_p=1 spectral peaks is less than 50%.

The use and/or disclosure, etc. of the contents of this document (or any part thereof) is subject to the restrictions referenced on the front page.

***if the relative number of Quality_n=1 spectral peaks is more than 30%

4.2.3.7 *Product variables characterizing the mean properties of the identified Pc1 events*

The mean properties of the identified Pc1 events are characterised by the product variables summarised in the following table.

Variable Name	Type	Dim	Unit	Description
ORB_m_C	CDF_UINT2	1	-	Orbit number for the Bp/Ba/Br component ID event (mean properties)
DIR_m_C	CDF_INT1	1	-	Flight direction for the Bp/Ba/Br component ID event (mean properties)
ID_m_C	CDF_UINT1	1	-	Bp/Ba/Br component event identifier for event mean properties
Timestamp_m_C	CDF_EPOCH	1	-	Mean time of observation for the Bp/Ba/Br component ID event, UTC
Latitude_m_C	CDF_DOUBLE	1	deg	Mean position in ITRF – Geocentric latitude for the Bp/Ba/Br component ID event
Longitude_m_C	CDF_DOUBLE	1	deg	Mean position in ITRF – Geocentric longitude for the v component ID event
Radius_m_C	CDF_DOUBLE	1	m	Mean position in ITRF – Geocentric radius (from the Earth centre) for the Bp/Ba/Br component ID event
Latitude_QD_m_C	CDF_DOUBLE	1	deg	Mean QD latitude for the Bp/Ba/Br component ID event
Longitude_QD_m_C	CDF_DOUBLE	1	deg	Mean QD longitude for the Bp/Ba/Br component ID event
MLT_m_C	CDF_DOUBLE	1	hr	Mean Magnetic Local Time for the Bp/Ba/Br component ID event
SZA_m_C	CDF_DOUBLE	1	deg	Mean Solar zenith angle for the Bp/Ba/Br component ID event

The use and/or disclosure, etc. of the contents of this document (or any part thereof) is subject to the restrictions referenced on the front page.

Variable Name	Type	Dim	Unit	Description
Duration_m_C	CDF_DOUBLE	1	min	Duration of the Bp/Ba/Br component ID event
Frequency_m_C	CDF_DOUBLE	1	Hz	Mean frequency for the Bp/Ba/Br component ID event
Freq_std_m_C	CDF_DOUBLE	1	Hz	Standard deviation of the spectral peak frequencies for the Bp/Ba/Br component ID event
Halfwidth_m_C	CDF_DOUBLE	1	Hz	Mean spectral peak half width for the Bp/Ba/Br component ID event
Power_m_C	CDF_DOUBLE	1	nT^2/Hz	Mean power for the Bp/Ba/Br component ID event
Prominence_m_C	CDF_DOUBLE	1	-	Mean prominence for the Bp/Ba/Br component ID event
ROFC_m_C	CDF_DOUBLE	1	Hz/s	Rate of frequency change for the Bp/Ba/Br component ID event
Quality_m_C	CDF_UINT1	1	-	Overall quality for the Bp/Ba/Br component ID event 0: high quality data 1: not nominal operation of the VFM instrument 2: low number of primary data points 3: contaminated spectra 4: 1 and 2 5: 1 and 3 6: 2 and 3 7: 1 and 2 and 3 (see [AD-2] for further details)

*The “Average rate of frequency change” is given as the slope of the linear fit of the spectral peaks.

The use and/or disclosure, etc. of the contents of this document (or any part thereof) is subject to the restrictions referenced on the front page.

4.2.3.8 *Saving the data in daily cdf product files*

Finally, all the product variables are written into daily cdf files. The name of the cdf files follow the Swarm convention [AD-4]. The file name has the format:

MM_CCCC_FFFxDDD_2z_yyyymmddThhmmss_YYYYMMDDTHHMMSS_vvvv.EXT,

where 'MM' stands for the mission identifier ('SW' for Swarm), 'CCCC' is the type of the product (e.g., 'OPER' for operational), 'FFFxDDD_2z' is the product name, 'yyyymmddThhmmss' and 'YYYYMMDDTHHMMSS' are the validity start and stop time (i.e., the time of the first and last data record in the file that is 00:00:00 and 23:59:59 for daily files), respectively, while 'vvvv' is the version number. For this product 'EXT' is always 'cdf'. The product name consists of the following elements: 'PC1' ('FFF') to identify the target of the product, followed by the identifier of the Swarm satellite ('A', 'B' or 'C'), 'DDD' is 'MAG' referring to the source data identifier, finally '2F' is used for '2z', indicating that this is a Level-2 Fast Track product. An example is given below:

SW_OPER_PC1AMAG_2F_20150402T000000_20150402T235959_0101.cdf

The content of the file is detailed in [AD-2], however, the variables are also listed in this document in Sections 4.1.3.6, 4.1.4.4, and 4.1.4.6.

Note that the processing algorithm is run whenever a half orbit is longer than 5 minutes, which means that PC1xMAG_2F may be available for days when the MAGx_HR record is incomplete.

4.2.3.9 *No event case*

PC1xMAG files are generated even when no events in some of the components or all components are detected. In this case the ORB, DIR and ID type variables are set to 0, Quality flags are all 254, while the Timestamp is 01-Jan-2000. The characterisation variables are all NaNs in such a case.

The use and/or disclosure, etc. of the contents of this document (or any part thereof) is subject to the restrictions referenced on the front page.

Summary

This document discusses the derivation of the two Swarm ULF products **ULFxMAG_2F** (Section 4.1), and **PC1xMAG_2F** (Section 4.2) in detail and also the background knowledge the products and their derivations are based on.

The use and/or disclosure, etc. of the contents of this document (or any part thereof) is subject to the restrictions referenced on the front page.